Jurnal Kejuruteraan 36(4) 2024: 1437–1450
https://doi.org/10.17576/jkukm-2024-36(4)-09

Electrochemical Performance of Activated Carbon Derived from Empty Fruit Bunch via Chemical and Physical Activation Method

Hasan Marzuki[a], Alya Naili Rozhan[a*] & Hadi Purwanto[b]

[a]*Kulliyyah of Engineering, International Islamic University Malaysia, Jalam Gombak, 53100 Kuala Lumpur Malaysia,*

[b]*UISI, Kompleks PT. Semen Indonesia, Jalan Veteran, Gresik Wast Java, 61122, Indonesia*

[*]*Corresponding author: alyanaili@iium.edu.my*

Received 17 January 2024, Received in revised form 21 March 2024
Accepted 21 April 2024, Available online 30 July 2024

ABSTRACT

Empty fruit bunch (EFB) is a promising materials to produce activated carbon for electrode materials applications in an energy storage device due to its low cost, high availability and porosity. EFB will require further processing to convert it into activated carbon to enhance its electrochemical performance. In this research, a two-step activation was utilized, in which EFB undergone pyrolysis at 500 °C before being activated via chemical and physical activation methods under various conditions to produce activated carbon. The samples were then characterized using weight loss analysis, Field Emission Scanning Electron Microscopy with Energy Dispersive X-ray Spectroscopy (FESEM-EDX) and Raman Spectroscopy to evaluate their physical characteristics. Cyclic voltammetry (CV), galvanostatic charge discharge (GCD) and electrochemical impedance spectroscopy (EIS) were performed to evaluate their electrochemical performance. The specific capacitance measured from CV analysis shows better performance for samples from physical activation which were in the range of 24 to 140 F/g compared to samples from chemical activation that resulted in only 36 to 90 F/g. These results suggested that physical activation has yielded better electrochemical performance of activated carbon which was influenced by the higher activation temperature in comparison with that of the chemical activation that was performed at lower activation temperature.

Keywords: Empty fruit bunch; activated carbon; chemical activation; physical activation; supercapacitor

INTRODUCTION

The development of renewable energy has emerged as a significant trend, driven by a growing societal awareness of climate change and global warming. This awareness has catalyzed a shift away from fossil fuel-based energy toward greener and more sustainable renewable energy resources. An essential consideration for the utilization of renewable energy resources is the need for an efficient energy storage system, given the intermittent availability of these sources (Shah et al. 2023). Currently, the energy storage system market is largely dominated by rechargeable batteries. However, the drawbacks of these systems, including low power density, short life cycles, and rapid capacity reduction, may not fully align with the demands of end-users (Chu et al. 2019). The shortcomings of rechargeable batteries have created opportunities for supercapacitors, which operate on the electric double layer mechanism, to emerge as promising alternatives. Supercapacitors offer high cycling stability, power density, and extended lifespan, making them a compelling choice in overcoming the limitations associated with traditional rechargeable batteries.

Supercapacitors are energy storage devices composed of electrodes, an electrolyte, and a current collector, offering a broad spectrum of energy and power density. The electrode, a crucial component of the supercapacitor, plays a pivotal role in governing the charging and discharging behavior. Consequently, it significantly influences the electrochemical performance of the supercapacitor as an energy storage device. There are three primary types of supercapacitors: electric double layer capacitor (EDLC), pseudocapacitor, and hybrid

supercapacitor (Mensha-Darkwa et al. 2019). The primary feature distinguishing these supercapacitors lies in their charging and discharging mechanisms, which are dictated by the behavior of their electrode materials. EDLC employs a carbon-based electrode, relying on its adsorption and desorption ability of electrolyte ions at the electrode-electrolyte interface. Pseudocapacitors operate through fast redox reactions facilitated by their metal oxide electrodes. In contrast, a hybrid supercapacitor combines both metal oxide and carbon-based electrodes, leveraging a synergistic blend of the charging and discharging mechanisms from each material.

Biomass materials characterized by a high carbon content have garnered attention as intriguing raw materials for the production of activated carbon-based electrodes in supercapacitors (Bujang et al. 2023 and Dolah et al. 2014). These attributes stem from their low cost, widespread availability, and inherent characteristics, including porosity and surface area, which render them ideal candidates for high-performance electrochemical energy storage devices (Al-Rajabi et al. 2022 and Najib et al. 2019). The synthesis of activated carbon involves an activation method conducted at elevated temperatures, employing activation agents such as CO_2, steam, zinc chloride ($ZnCl_2$), phosphoric acid (H_3PO_4) and potassium hydroxide (KOH) (Sahsiny et al. 2021). Table 1 presents the electrochemical performance of activated carbon derived from biomass alongside conventional carbon materials such as graphite, petroleum coke, and carbon nanotubes (CNT). Notably, the majority of the activation processes were carried out at temperatures exceeding 700 °C, regardless of whether the carbon source was biomass-based or conventional. Upon comparing their electrochemical performance, there is no substantial value differential between biomass-based carbon and conventional carbon materials. This suggests that activation parameters, including temperature and activating agents, play pivotal roles in achieving high electrochemical properties for activated carbon, regardless of whether it is derived from biomass or conventional carbon sources.

TABLE 1. Electrochemical of Activated Carbon Derived from Biomass and Conventional Carbon Materials

Reference	Raw Material	Activation Method/ Agents	Activation Temperature (°C)	Specific Capacitance (Fg^{-1})
Farma et al. 2013	Green monolith of EFB and CNT	Physical activation (CO_2)	800	28.00 – 358.00
Sim et al. 2015	Food waste	Chemical activation (H_3PO_4)	700	45.00 – 85.00
Zhi et al. 2014	Waste tire	Chemical activation (H_3PO_4)	900	24.00 – 80.00
Awitdrus et al. 2016	Mix of EFB and green coke petroleum	Physical activation (CO_2)	800	6.50 – 82.50
Shabeeba et al. 2018	Charcoal	Physical activation (steam)	1400	65.00 – 70.00
Wei et al. 2016	Pollen grain	Physical activation (CO_2)	900	25.00 – 250.00
Hu et al. 2014	Alkali lignin	Chemical activation	850	67.00 – 344.00
Barzegar et al. 2017	Conventional carbon (Graphite)	Chemical activation (KOH)	800	337.00
Shi et al. 2018	Hemp straw	Chemical activation (KOH)	800	167.80 – 244.80
Choi et al. 2018	EFB	Chemical activation (KOH)	800	216.70 – 439.10
Nor et al. 2017	Mixture of EFB and graphite	Physical activation (CO_2)	800	20.00 – 80.00
Ishak et al. 2015	Mixture of EFB and CNT	Physical activation (CO_2)	800	5.75 – 113.33
Kanjana et al. 2021	Rubber seed shell, durian shell and palm petiole	Chemical activation (KOH)	800	123 - 178
Taer et al. 2021	Leaf waste	Physical activation (CO_2)	900	99 -168
Vinayagam et al. 2021	Soap nut seeds	Physical activation (CO_2)	700	138

Hence, this research entails a comparison of two activation methods: physical and chemical activation, employing local Malaysian biomass, specifically empty fruit bunch (EFB). CO2 gas will serve as the activating agent for physical activation, while KOH will be utilized for chemical activation. The choice of CO2 and KOH as activation agents is primarily attributed to the endothermic nature of their reactions with the carbon surface. This characteristic facilitates the activation process and contributes to lower energy consumption. (Pallares et al. 2018). Moreover, numerous studies have indicated that the utilization of these two activation agents may result in enhanced properties of the activated carbon (Hui et al. 2015). The focal point of this research is to showcase the assessment of distinct clusters of parameters through the application of different activation methods. Chemical activation will involve variations in activation agent concentrations at a constant temperature. Conversely, physical activation will entail diverse activation temperatures with a consistent activation agent. Additionally, this study delves into exploring the research gap related to activation processes conducted at lower temperatures, such as 500 °C, and their impact on the electrochemical properties of activated carbon.

METHODOLOGY

EXPERIMENTAL

The raw materials used in this study are empty fruit bunch (EFB), collected at Malaysian Palm Oil Board (MPOB), Bangi and preliminary characterization on EFB involved proximate and ultimate analysis to assess the elemental composition and overall components of the raw EFB. The EFB underwent crushing and drying in an oven at 105 °C for 24 hours. Subsequently, the dried EFB underwent a two-step activation process for the synthesis of activated carbon. Initially, the EFB was pyrolyzed to convert it into bio-char, followed by activation to produce activated carbon. The pyrolysis process was conducted at a temperature of 500 °C with a heating rate of 10 °C/min for 1 hour under Argon gas flow. Two types of activation were performed in this study: physical activation and chemical activation. For physical activation, the bio-char was subjected to heating at temperatures of 500 °C, 600 °C, 700 °C, 800 °C, and 900 °C, with a heating rate of 10 °C/min for 1 hour under CO_2 flow at 0.3 L/min, acting as the oxidizing agent in the activation process. In the case of chemical activation, the bio-char samples were impregnated with KOH at weight ratios of KOH to bio-char of 1:1, 2:1, 3:1, 4:1, and 5:1. Subsequently, the impregnated bio-chars were heated at a temperature of 500 °C with a heating rate of 10 °C/min for 1 hour under flowing Argon. The samples for chemical and physical activation were denoted as AC 1:1, AC 2:1, AC 3:1, AC 4:1, and AC 5:1, and AC 500, AC 600, AC 700, AC 800, and AC 900, respectively.

PHYSICAL CHARACTERIZATION

Weight loss analysis, Raman spectroscopy and Field Emission Scanning Electron Microscopy with Energy Dispersive X-Ray Spectroscopy (FESEM-EDX) were carried out to evaluate the physical properties of activated carbon.

The weight of the sample was measured at each stage of experimental process such as before pyrolysis, after pyrolysis, before activation and after activation. The weight loss measurement is crucial as it provides a better understanding of the process mechanism and establishes correlations with other characterization results. Raman spectroscopy analysis was carried out using Reinshaw inVia confocal Raman spectrometer with 532 nm excitation laser to investigate the defect structure of the activated carbon materials by evaluating the ratio of the I_D/I_G on the Raman spectra. FESEM-EDX analysis was carried out using FESEM-ZEISS Supra 55VP instrument to evaluate the composition of activated carbon. FESEM analysis was conducted at 50,000 magnification with electron high tension of 10 kV and working distance of 3.6mm between the lens and the specimen surface.

PREPARATION OF ELECTRODE

The slurry was prepared by combining activated carbon as the active material, graphite as the conductive additive, and polytetrafluoroethylene (PTFE) as the binder in an 8:1:1 ratio. The mixture was stirred to achieve homogeneity of the slurry. Stainless steel mesh, cut into 1 cm by 1 cm pieces, served as the current collector. Subsequently, 0.01 g of the slurry was applied to the current collector and hot-pressed at 10 MPa and 80 °C.

ELECTROCHEMICAL ANALYSIS

The electrochemical measurements were carried out using Metrohm Autolab electrochemical workstation in three electrode configuration, with activated carbon electrode being the working electrode, graphite as the counter electrode and Ag-Ag/Cl as the reference electrode in a 6M KOH aqueous solution. The potential window of the cyclic voltammetry (CV) test was conducted from -0.8 to 0.4 V using scan rates of 2 – 20 mV/s with increments of 2 mV/s. The specific capacitance calculated from CV test using Equation 1 (Mensah-Darkwa et al. 2019):

$$C_p = \frac{A}{2mk(\Delta V)} \quad (1)$$

Where, Cp is specific capacitance, A is area inside CV curve, m is mass of activated carbon, k is scan rate and ΔV is potential window.

The voltage range of galvanostatic charge and discharge (GDC) test was -0.8 to 0.1 V with current density of 0.1 A/g. The specific capacitance, energy density and power density calculated from GCD test using Equation 2 to Equation 4 below (Mensha-Darkwa et al. 2019):

$$C_p = \frac{A}{2mk(\Delta V)} \quad (2)$$

$$C_p = \frac{I}{m\frac{dV}{dt}} \quad (3)$$

$$P = \frac{3.6E}{\Delta t} \quad (4)$$

Where, Cp is specific capacitance, I is current, m is mass of activated carbon, $\frac{dV}{dt}$ is discharge slope of GCD curve, E is energy density, V is potential window, P is power density and Δt is discharge time for GCD curve (Mensah-Darkwa et al. 2019).

Electrochemical impedance spectroscopy (EIS) test was performed with frequency of 100 kHz to 10 mHz with an amplitude of 10 mV.

RESULTS AND DISCUSSION

PRELIMINARY CHARACTERIZATION OF EFB

EFB is a lignocellulosic biomass composed primarily of carbon, oxygen, and hydrogen as its main elemental components. Concurrently, the gross components of EFB include fixed carbon, volatile matter, moisture, and ash. Table 2 below provides the proximate and ultimate analysis, illustrating the composition of elemental and gross components of EFB.

As depicted in Table 2, EFB exhibited a substantial amount of volatile matters. These volatile matters play a crucial role in generating porous structural networks. During the pyrolysis process, these volatile matters undergo vaporization, leaving behind a network of pores within the bio-char. Subsequent to the activation process, the interaction between the activation agents, CO_2 and KOH with the bio-char surfaces led to the opening of initially inaccessible pores, forming an additional pore structure characterized by smaller pore sizes.

TABLE 2. Proximate and Ultimate Analysis

Proximate Analysis	(wt%.)	Ultimate Analysis	(wt%.)
Fixed Carbon	8.98	Carbon	45.64
Volatile Matter	83.94	Oxygen	47.82
Moisture	6.80	Hydrogen	6.19
Ash	7.08	Sulfur	0.35

PHYSICAL CHARACTERIZATION OF EFB

The mechanism of the two-step activation process for the conversion of EFB to activated carbon is illustrated in Figure 1. The process initiates with the pyrolysis of EFB, transforming it into bio-char. During this heating phase, volatile matters in the EFB undergo devolatilization, leading to the creation of a porous structure within the bio-char (Purwanto et al. 2018). Subsequently, during the activation process, the bio-char undergoes further heating, during which CO_2 and KOH create a new structure comprising mesopores (pore size of 2-50 nm) and micropores (pore size less than 2 nm) (Ilomuanya et al. 2016). The development of this pore network has augmented the specific surface area and pore volumes, playing pivotal roles in enhancing the performance of the energy storage device. The reactions between CO_2 and bio-char, as well as between KOH and bio-char, are described in Equation 5 and Equation 6 to Equation 8, respectively (Lan et la., 2019, Mopoung et al. 2015).

$$CO_2 + C \rightarrow 2CO \quad (5)$$

$$4KOH + C \rightarrow K_2CO_3 + K_2O + 2H_2 \quad (6)$$

$$K_2CO_3 + 2C \rightarrow 2K + 3CO \quad (7)$$

$$K_2O + C \rightarrow 2K + CO \quad (8)$$

As illustrated in Equation 5, CO_2 reacts with bio-char (carbon), releasing CO and consuming carbon in the process, thereby creating pores within the bio-char. Similarly, the reaction between KOH and bio-char results

in the release of K_2CO_3 and K_2O. These compounds subsequently react with bio-char, producing CO gas and K atoms. These reactions also consume carbon, leading to the formation of networks of pores inside the activated carbon (Reza et al. 2020).

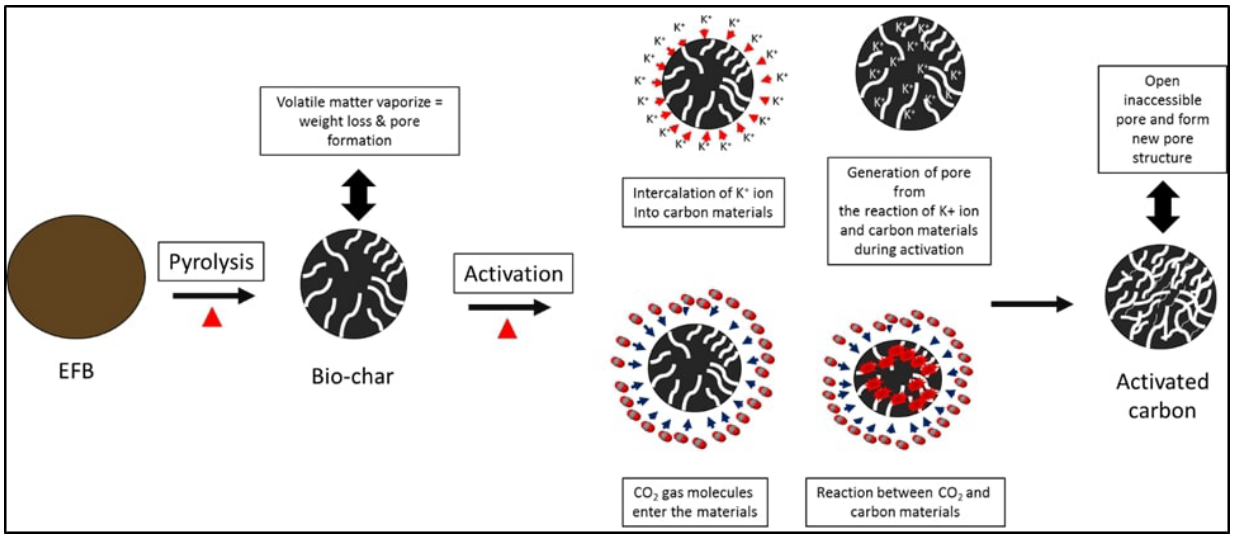

FIGURE 1. Mechanism of EFB conversion to activated carbon via two-step activation method

Table 3 provides an overview of the weight loss analysis for the conversion of EFB to bio-char and the subsequent conversion of bio-char to activated carbon.

The weight loss observed after the pyrolysis process primarily results from the removal of volatile matters. Subsequent weight loss during activation occurs due to the reaction between bio-char (carbon) and the activating agent. It is evident that samples subjected to physical activation exhibit higher weight loss compared to those undergoing chemical activation. This trend is particularly notable for the physical activation samples exposed to 800 °C and 900 °C.

TABLE 3. Weight Loss Analysis

Sample	Weight Loss After Pyrolysis (%)	Weight Loss After Activation (%)
AC 1:1	65.5	10.9
AC 2:1	65.3	13.0
AC 3:1	66.0	6.6
AC 4:1	65.8	5.8
AC 5:1	66.0	5.2
AC 500	64.0	9.7
AC 600	70.6	17.7
AC 700	71.2	17.3
AC 800	66.6	30.7
AC 900	69.6	54.3

The weight loss analysis suggests that higher activation temperatures lead to increased weight losses, as more volatiles are gasified from the bio-char bodies, contributing to the formation of more porous networks. Conversely, a high concentration of activation agent alone is insufficient to escalate the rate of activation reaction, resulting in low weight loss in samples such as AC 5:1. This is attributed to the insufficient energy supplied, hindering the acceleration of the activation reaction, evident in the weight loss observed during chemical activation (Olivares-Marin et al. 2012).

Furthermore, it can be inferred that some residual K+ ions may remain after the chemical activation reaction. This inference aligns with the weight loss analysis above, where an increase in sample weight is observed with an increase in the weight ratio of the chemical. This phenomenon is attributed to the low activation temperature, which leaves some K+ ions unused during the reaction, masking the weight loss associated with the removal of carbon species. In contrast, during physical activation, the elevation of activation temperature, while keeping the activation gas supply constant, results in more substantial consumption of carbon species due to the heightened reaction rate between CO_2 gas and the carbon surface. Consequently, higher weight loss is recorded for samples exposed to higher activation temperatures (Thongpat et al. 2021).

In Figure 2, FESEM images reveal the porous structure of the activated carbon surfaces across all samples, indicating the effectiveness of the activation process. Notably, Figure 2b showcases the sub-porous structure

within the surface porosity of AC 800, highlighting the hierarchical nature of the porous network. In contrast, other samples lack clear indications of this hierarchical pore structure. This distinction may be attributed to the higher activation temperature for AC 800 (800 °C) compared to AC 500, AC 1:1, and AC 2:1, which undergo activation at 500 °C. The elevated temperature implies increased energy input during the activation process, fostering higher reactivity and the formation of enhanced porosity and a hierarchical pore structure. The higher porosity and the formation of a hierarchical structure within the activated carbon facilitate the movement of electrolyte ions within the pore network. This, in turn, enhances the efficiency of utilizing the specific surface area of the activated carbon, resulting in superior electrochemical properties. (Wang et al. 2023). Furthermore, it is evident that physical activation samples exhibit smoother textures compared to chemical activation samples. This difference is attributed to potential residual KOH remaining on the surface of the activated carbon, giving rise to cavities and impurities. This observation aligns with the reactions described in Equation 6 to Equation 8, where the reaction products may contribute to the surface irregularities observed in the chemical activation samples. (Arango et al. 2018 and Madzaki et al. 2018).

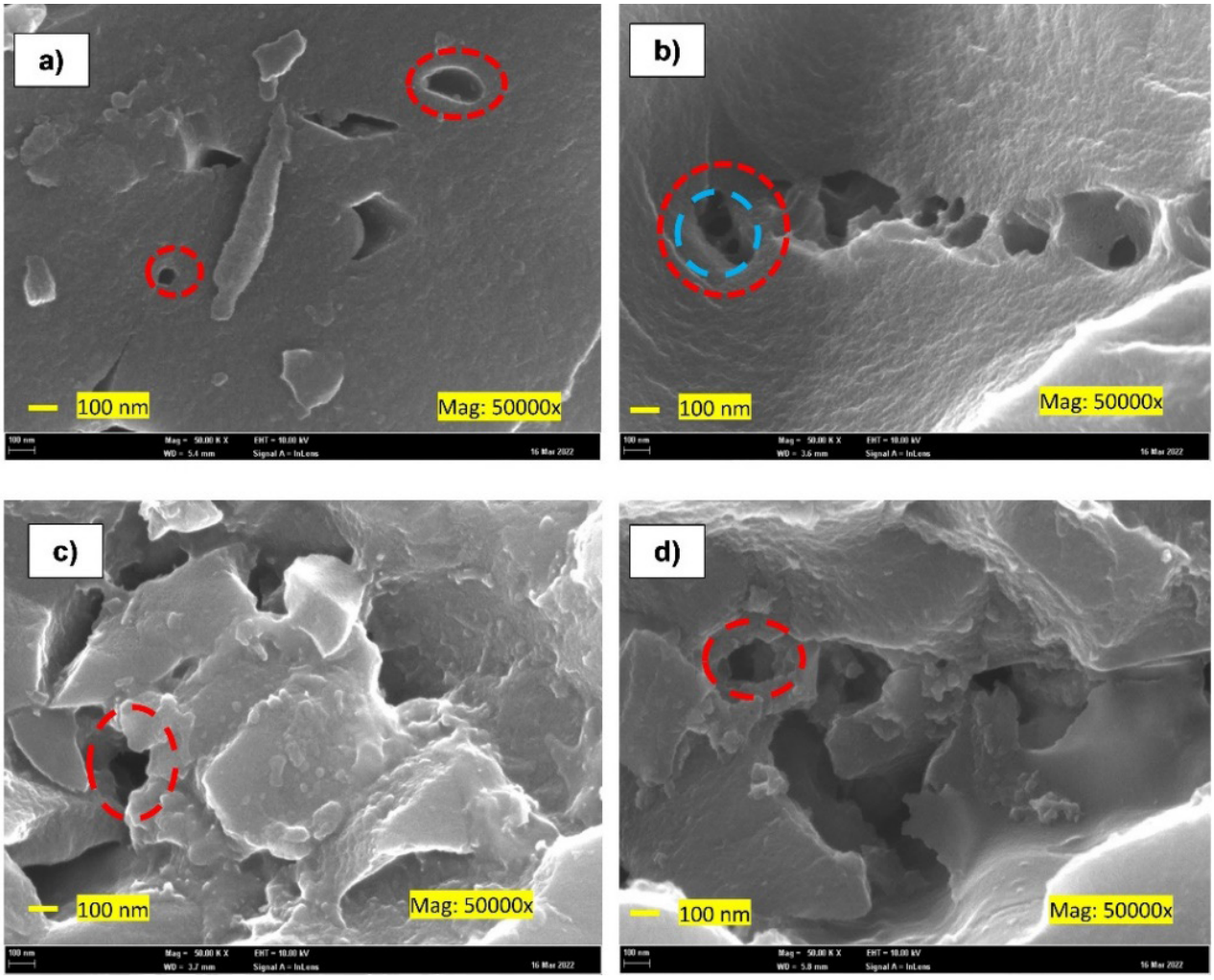

FIGURE 2. FESEM images for a) AC 500 b) AC 800, c) AC 1:1 and d) AC 2:1

Table 4 provides the elemental composition for selected activated carbon samples using EDX analysis. When compared to the elemental compositions of raw EFB in Table 2, all samples exhibit an increase in carbon content. Notably, AC 800 boasts the highest carbon content and the lowest oxygen content among the samples. This aligns with the weight loss analysis, suggesting that the activation process yield carbon content and reduces oxygen content (Mahmud et al. 2018).

TABLE 4. EDX Analysis

Sample	Carbon (wt%.)	Oxygen (wt%.)	Nitrogen (wt%.)
AC 1:1	80.5	8.5	0.3
AC 2:1	80.1	15.5	2.8
AC 500	84.7	8.5	1.2
AC 800	88.5	6.6	1.5

Figure 3 depicts the Raman spectroscopy analysis of the activated carbon. In the context of energy storage device applications, characterizing defects in activated carbon materials is crucial. The presence of a higher defect structure can increase the density of electronic states in the carbon materials, subsequently enhancing the capacitance of the carbon materials (Zheng et al. 2021). Analysis of defects in carbon materials can be conducted through the examination of the ID and IG values in the Raman spectra. A higher ID/IG ratio signifies a greater defect structure within the carbon materials. Specifically, the D and G bands corresponding to the activated carbon are observed at 1341 cm^{-1} and 1600 cm^{-1}, respectively (Bonhomme et al. 2001).

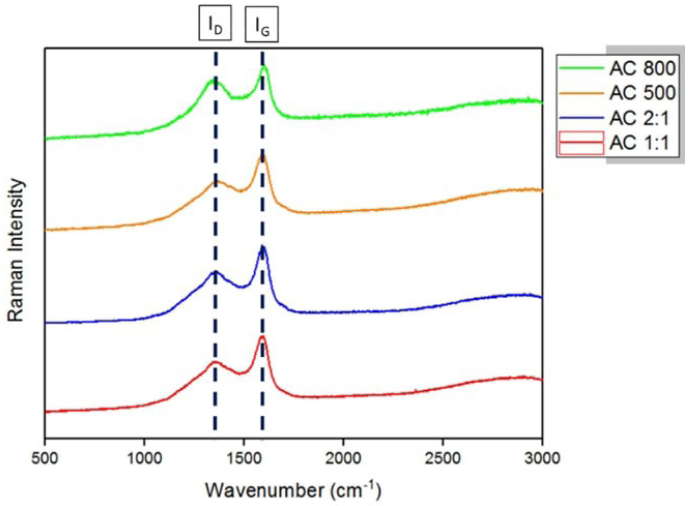

FIGURE 3. Raman Spectroscopy Analysis

Table 5 presents the I_D/I_G values for the activated carbon samples. As previously mentioned, a higher ID/IG value indicates a greater defect structure, which is expected to lead to an increase in the specific capacitance of the activated carbon. However, it's important to note that this relationship is not always straightforward, as other factors, such as porosity and surface area, can also influence the specific capacitance of carbon materials. Referring to Table 5, AC 800 exhibits a higher defect structure compared to the other samples, which have approximately similar values. This finding aligns with the weight loss analysis discussed earlier, revealing that activation at a higher temperature resulted in increased weight loss due to the reaction between the activation agent and the carbon materials. AC 800, having a higher weight loss, indicates the formation of more defect/pore structures during the activation process. Consequently, the AC 800 sample exhibits a higher I_D/I_G value.

TABLE 5. I_D/I_G for Activated Carbon Sample

Sample	I_D/I_G
AC 1:1	0.71
AC 2:1	0.70
AC 500	0.70
AC 800	0.84

The defect structure identified through Raman spectroscopy correlates with the weight loss analysis discussed earlier. The weight loss of the sample during the activation process serves as an indicator of the reactivity between the activation agent and the carbon surface. Higher reactivity implies that more carbon species react with the activation agent, leaving behind a porous structure. This, in turn, translates into the formation of defect structures within the activated carbon sample (Farma et al. 2013).

ELECTROCHEMICAL PERFORMANCE ANALYSIS

In Figure 4c) and d), the CV analysis was conducted using several scan rates, revealing a decrease in specific capacitance values with the increase in scan rate. Meanwhile, Figures 4a) and b) provide a comparison between CV curves for different samples at the same scan rate. The area under the curve in these figures indicates the specific capacitance performance of the activated carbon—larger areas correspond to higher specific capacitance. Figure 4 illustrates the CV analysis for activated carbon produced via both physical and chemical activation methods.

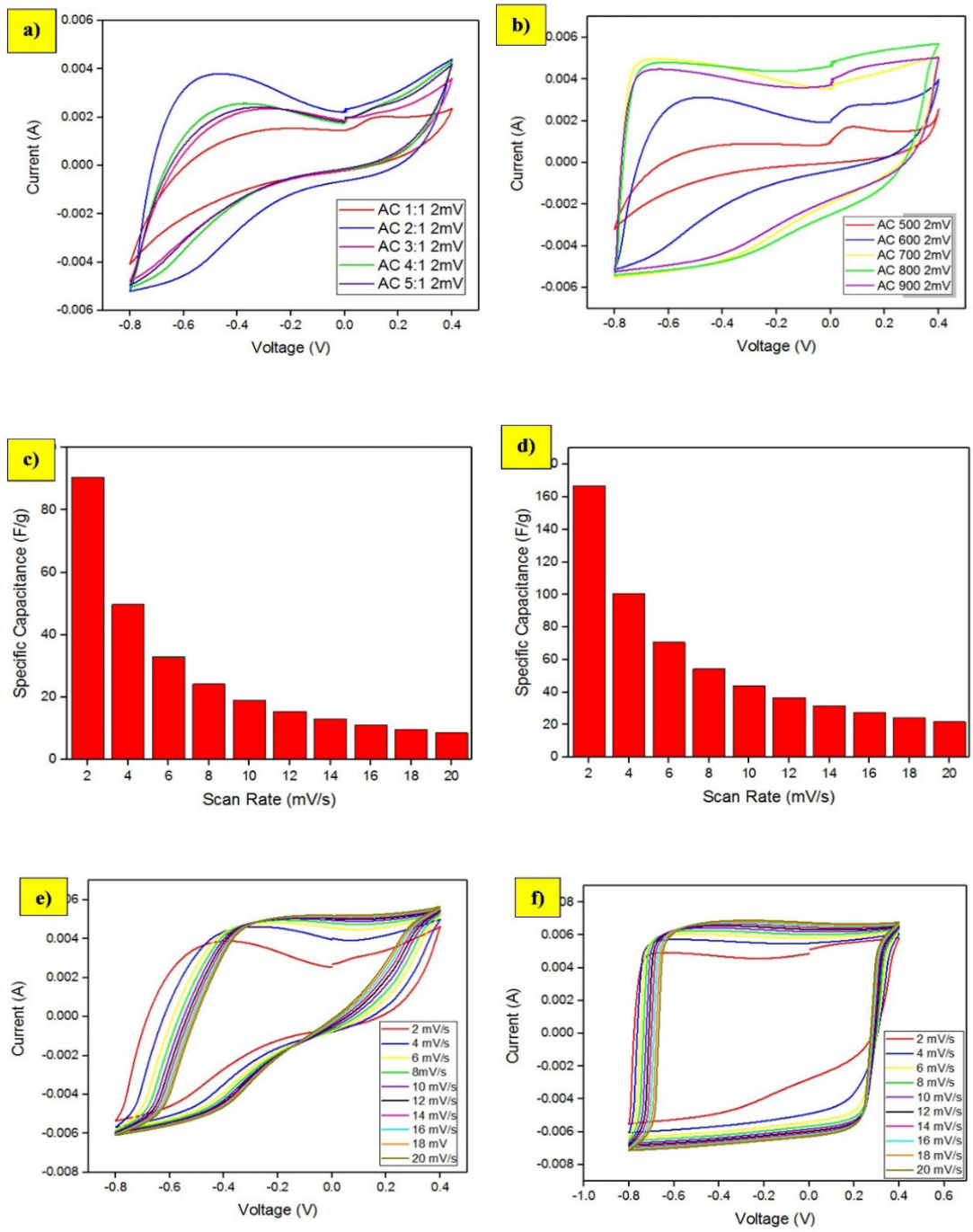

FIGURE 4. CV analysis for a) chemical activation samples b) physical activation samples, and specific capacitance for c) AC 2:1 d) AC 800, CV analysis for various scan rates for e) AC 2:1 f) AC 800

Table 6 displays the specific capacitance values calculated using Eq. 1 based on the CV curves in Figure 4. Overall, the activated carbon samples synthesized via physical activation demonstrate better specific capacitance compared to those obtained through chemical activation.

TABLE 6. Specific Capacitance of Activated Carbon Electrode

Sample	Specific Capacitance, C_P (F/g)
AC 1:1	36.80
AC 2:1	90.54
AC 3:1	52.03
AC 4:1	59.81
AC 5:1	54.82
AC 500	24.72
AC 600	76.00
AC 700	146.60
AC 800	166.80
AC 900	140.27

The trends observed in specific capacitance align with the physical properties of the activated carbon samples. For activated carbon subjected to physical activation, there is an increasing trend in specific capacitance with rising temperature. In contrast, activated carbon undergoing chemical activation shows a decreasing trend in specific capacitance with the increase in the concentration of the impregnated activation agent within the bio-char. As discussed earlier, the weight loss analysis revealed that physical activation samples had higher reactivity, leading to the development of a more extensive porous network within the activated carbon. This observation is further supported by the FESEM analysis, which indicates that AC 800 developed a hierarchical porous structure in comparison to other samples due to its higher reactivity and weight loss during the activation process. In connection with specific capacitance, it is evident that AC 800 exhibits the highest specific capacitance compared to others. This can be attributed to the high reactivity during the activation process, resulting in the development of a hierarchical porous structure. This structure significantly facilitates ion movement within the porous network, thereby contributing to superior electrochemical performance (Yang et al. 2018).

Furthermore, the defect structure of the activated carbon material appears to influence its specific capacitance, as discussed earlier. The defect structure, characterized by the ID/IG values from the Raman spectroscopy analysis (Figure 3 and Table 5), exhibits consistency with the specific capacitance results. Specifically, AC 800, with a higher defect structure, demonstrates a higher specific capacitance value compared to other samples. Although the defect structure may not be the sole determinant of specific capacitance, it undeniably contributes to the enhancement of the electrochemical performance of the activated carbon.

In Figure 5b), c), and d), Nyquist plots obtained through EIS analysis are presented. These plots enable the determination of the resistance values of the activated carbon. The resistance values were derived by examining the semicircle portion in the Nyquist plot, providing information on the electrolyte resistance when in contact with the electrode (R_S), the internal resistance of the activated carbon electrode (R_P), and the equivalent series resistance (ESR) of the activated carbon electrode. The values of R_S, R_P, and ESR are represented by the beginning of the semicircle line, the termination of the semicircle line, and the diameter of the semicircle ($R_P - R_S$), respectively (Farma et al. 2013). The corresponding values of R_P, R_S, and ESR are detailed in Table 7.

TABLE 7. EIS Analysis

Sample	R_S (Ω)	R_P (Ω)	ESR (Ω)
AC 1:1	2.67	122.82	120.15
AC 2:1	2.66	20.08	17.43
AC 3:1	2.88	49.24	46.36
AC 4:1	2.84	51.45	48.61
AC 5:1	2.53	43.35	40.82
AC 500	2.60	156.56	153.96
AC 600	2.77	21.73	18.96
AC 700	2.66	3.91	1.25
AC 800	4.04	4.14	0.10
AC 900	3.16	3.94	0.78

The values presented in Table 7 align with the earlier discussion on specific capacitance, where higher resistance values correspond to lower specific capacitance. Several factors contribute to the resistance value, including surface area, porosity, defect structure, and the presence of functional groups. Furthermore, the Equivalent Series Resistance (ESR) value can serve as an indicator for the behavior of the carbon-based supercapacitor. It is reported that the typical ESR value for a carbon electrode supercapacitor falls within the range of 0.134 to 1.149 (Kim et al. 2006). The presented values are consistent with activated carbon synthesized at high temperatures, such as AC 800 and AC 900. These samples exhibit higher resistance values, which align with the trend observed in the specific capacitance results and suggest the influence of synthesis conditions on the electrochemical performance of the activated carbon.

The straight line following the semicircle in the Nyquist plot represents the resistive and capacitive behaviors of ions penetrating the pore networks of the

activated carbon. A steep slope in this line indicates efficient penetration of ions into the activated carbon pores (Chen et al. 2003). The Nyquist plots for AC 700, AC 800, and AC 900 exhibit very steep slopes compared to other samples, indicating higher penetration of ions into their pore networks. This efficient ion penetration results in higher specific capacitance generation. Among the activated carbon samples synthesized via chemical activation, AC 2:1 shows the steepest slope, leading to the highest specific capacitance among the chemical activation samples.

Figure 5a) illustrates the GCD curve for samples AC 800 and AC 2:1. The GCD curve can be segmented into two phases: the increasing slope represents the charging process, while the decreasing slope represents the discharging process. Higher charging and discharging times indicate greater involvement of electrolyte ions in the charging and discharging process. Observing the data in Table 7, it is evident that AC 800, with higher charging and discharging frequencies, demonstrates better electrochemical performance compared to AC 2:1. This indicates that AC 800 has a higher specific capacitance and more efficient charge/discharge processes, which contribute to its superior electrochemical performance.

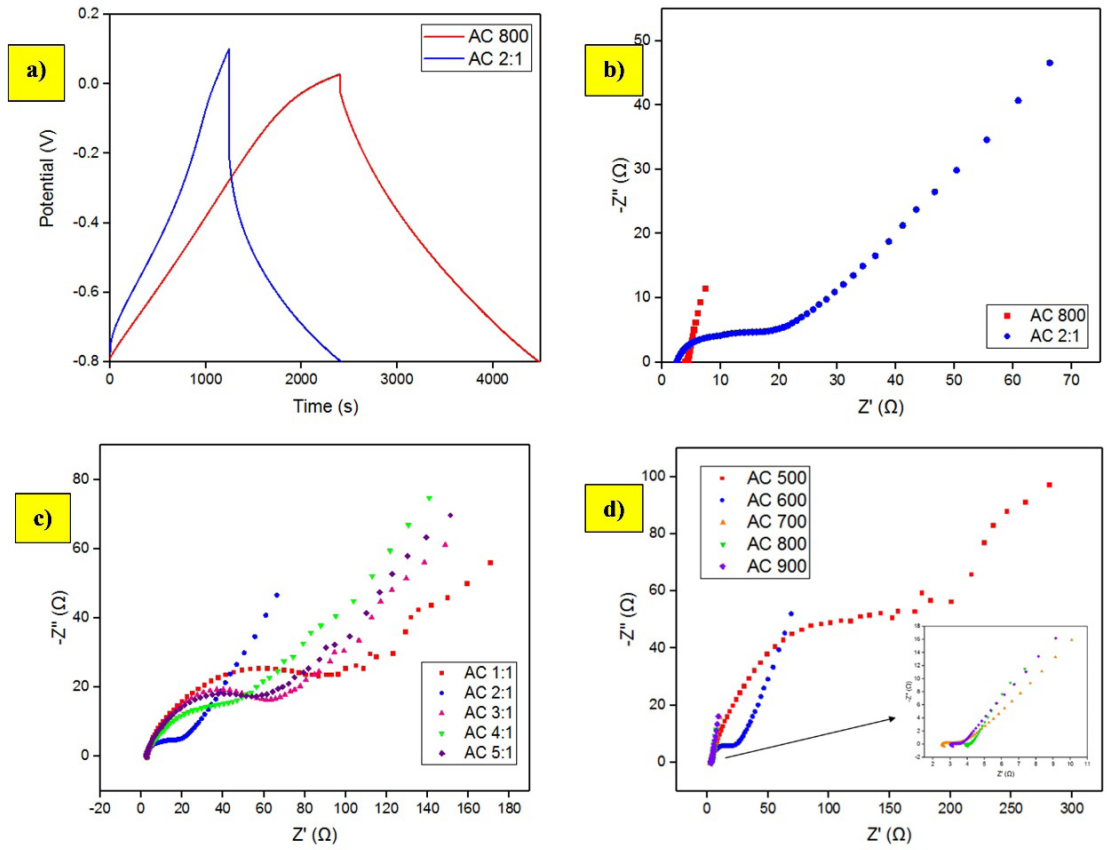

FIGURE 5. a) GCD analysis for AC 2:1 and AC 800, b) EIS analysis comparison for AC 2:1 and AC 800, c) EIS analysis for chemical activation sample d) EIS analysis for physical activation sample

The sharp drop in the initial voltage upon discharge for both AC 800 and AC 2:1 indicates diffusion-limited mobility of the electrolyte ions within the activated carbon pore network. This phenomenon suggests that the ions face constraints in moving through the pores during the discharge process, influencing the electrochemical behavior of the supercapacitor (Yu et al. 2011). The limitation in diffusion-limited mobility, as indicated by the sharp drop in voltage upon discharge, is associated with the ESR value of the activated carbon electrode. The higher sharp drop in voltage for AC 2:1 compared to AC 800 suggests that AC 2:1 experiences higher diffusion-limited mobility. This observation aligns with the obtained ESR values, further confirming the influence of ESR on the diffusion behavior in the supercapacitor.

Table 8 shows specific capacitance, energy density and power density that have been calculated from the GCD curve in Figure 6 a) using Eq. 2, 3 and 4.

TABLE 8. Electrochemical Performance of Activated Carbon Electrode from GCD Analysis

Sample	Specific Capacitance from GCD (F/g)	Energy Density (Wh/kg)	Power Density (W/kg)
AC 2:1	195	35	108
AC 800	255	85	147

The comparison of energy density and power density between the activated carbon synthesized using chemical activation and physical activation aligns with the electrochemical performance evaluated using EIS. Additionally, the energy density of AC 800, a biomass-based carbon electrode, demonstrates a relatively good value compared to numerous studies reporting energy density in the range of 2.95 to 4.43 Wh/kg. This suggests that AC 800 exhibits competitive energy storage capabilities within the reported range (Taer et al. 2016, Nor et al. 2017, Ishak et al. 2015). As for power density, the recorded value for AC 800 is slightly lower than in previous studies on biomass-based carbon electrodes. Nevertheless, the value remains relatively comparable, considering that power density in previous studies on biomass-based carbon electrodes is reported to be in the range of 150 to 620 W/kg. This suggests that AC 800 maintains competitive power storage capabilities within the reported range (Ishak et al. 2015, Deraman et al. 2011; Barzegar et al. 2017).

CONCLUSION

This work demonstrates the comparison between two types of activation methods which are chemical activation and physical activation. Both methods were conducted by using different clusters of parameters. In the chemical activation process, different concentration of activation agent, KOH, were being used with a constant activation temperature. Meanwhile, for physical activation, the effects of the activation temperature on the properties of the activated carbon produced have been studied under a constant flow of activation gas, CO_2.

1. The weight loss analysis has shown that the reaction rate of the physical activation is higher due to more weight loss during activation process compared to the chemical activation.
2. Raman spectroscopy analysis shows that the activation temperature plays significant roles in the development of the defect structure within the activated carbon which is in line with the weight loss analysis. (Just mention the I_D/I_G.)
3. Three electrochemical tests have been performed which are CV, GCD and EIS. The CV analysis indicates that AC 800 exhibits the highest specific capacitance at 166.80 F/g. This superior performance can be attributed to the physical properties of the sample, particularly the formation of a porous and defect structure under the specified activation parameters. The consistency observed in EIS and GCD analyses further supports the specific capacitance findings from the CV analysis.

Hence, from this study it can be concluded that activation temperature plays an important role over the concentration of the activation agent in synthesizing activated carbon that could give better electrochemical performance.

ACKNOWLEDGEMENT

This research is supported by Ministry of Higher Education Malaysia through Fundamental Research Grant Scheme, FRGS/1/2019/TK07/UIAM/03/3.

DECLARATION OF COMPETING INTEREST

None

REFERENCES

Al-Rajabi, M.M. and Haan, T.Y. 2022. Green extraction method of cellulose fibers from oil palm empty fruit bunches. *Jurnal Kejuruteraan* 34(5): 851-860. DOI: https://doi.org/10.17576/jkukm-2022-34(5)-12

Arango, D.I., Zapata-Benabithe, Z., Arenas, E.C., and Perez-Osorno, J.C. 2018. Influence of surface modification with nitric acid on electrochemical performance of agroindustrial waste-based activated carbon. *Journal of Materials Science: Materials in Electronics* 29(18): 15557-15569. DOI: https://doi.org/10.1007/s10854-018-9132-y

Awitdrus, A., 2016. Cyclic voltammometry of binderless activated carbon monoliths based supercapacitor from mixtures of pre-carbonized of fibers of empty fruit bunches and green petroleum coke. *KnE Engineering* 1(1). DOI: https://doi.org/10.18502/keg.v1i1.511

Barzegar, F., Bello, A., Dangbegnon, J.K., Manyala, N., and Xia, X. 2017. Asymmetric carbon supercapacitor with activated expanded graphite as cathode and pinecone tree activated carbon as anode materials.

Energy Procedia 105:4098-4103. DOI: https://doi.org/10.1016/j.egypro.2017.03.869

Bonhomme, F., Lassegues, J.C., and Servant, L. 2001. Raman spectroelectrochemistry of a carbon supercapacitor. *Journal of the Electrochemical Society* 148(11): E450-E458. DOI: https://doi.org/10.1149/1.1409546

Bujang, M., Bakie, N.A., Bujang, U.H., Kian, L.S., Jusli, E.A., and Azahar, W.N.A.W. 2023. Characteristics of oil palm fruit ash as binderin asphaltic concrete. *Jurnal Kejuruteraan* 35(4): 913-921. DOI: https://doi.org/10.17576/jkukm-2023-35(4)-13

Chen, W.C., Wen, T.C., and Teng, H. 2003. Polyaniline-deposited porous carbon electrode for supercapacitor. *Eletrochimica Acta*. 48(6): 641-649. DOI: https://doi.org/10.1016/S0013-4686(02)00734-X

Choi, M.S., Park, S., Lee, H. and Park, H.S. 2018. Hierarchically nanoporous carbons derived from empty fruit bunches for high performance supercapacitors. *Carbon Letters* 25: 103-112. DOI: https://doi.org/10.5714/CL.2018.25.103

Chu, M., Li, M., Han, Z., Cao, J., Li, R., and Cheng, Z. 2019. Novel biomass-derived smoke-like carbon as a supercapacitor electrode materials. *Royal Society Open Science* 6: 190132. DOI: https://doi.org/10.1098/rsos.190132

Deraman, M., Ishak, M.M., Farma, R., Awitdrus, Taer, E., Talib, I.A., and Omar, R. 2011. Binderless composite electrode monolith from carbon nanotube and biomass carbon activated by H_2SO_4 and CO_2 gas for supercapacitor. *AIP Conference Proceedings* 1415(1). DOI: https://doi.org/10.1063/1.3667250

Dolah, B.N.M., Deraman, M., Othman, M.A.R, Farma, R., Taer, E., Awitdrus, Basri, N.H., Talib, I.A., Omar, R., and Nor, N.S.M. 2014. A method to produce binderless supercapacitor electrode from biomass carbon and carbon nanotubes. *Materials Research Bulletin* 60: 10-19 DOI: https://doi.org/10.1016/j.materresbull.2014.08.013

Farma, R., Deraman, M., Awitdrus, Talib, I.A., Omar, R., Manjunatha, J.G., Ishak, M.M., Basri, N.H., and Dolah, B.N.M. 2013. Physical and electrochemical properties of supercapacitor electrodes derived from carbon nanotube and biomass carbon. *International Journal of Electrochemical Science* 8(2013): 257-273. DOI: https://doi.org/10.1016/S1452-3981(23)14018-1

Hu, S., Zhang, S., Pan, N. and Hsieh, Y.L. 2014. High energy density supercapacitors from lignin derived submicron activated carbon fibers in aqueous electrolytes. *Journal of Power Sources* 270: 106-112. DOI: https://doi.org/10.1016/j.jpowsour.2014.07.063

Hui, T.S., and Zaini, M.A.A. 2015. Potassium hydroxide activation of actiated carbon: A commentary. *Carbon Letters*. 16(4): 275-280. DOI: http://dx.doi.org/10.5714/CL.2015.16.4.275

Ilomuanya, M.O., Billa, N., Ifudu, N.D., and Igwilo, C.I. 2016. The effect of pore size and morphology of activated charcoal prepared from midribs of Elaeis guineensis on adsorption of poisons using metronidazole and Escherichia coli O157:H7 as a case. *Journal of Microscopy and Ultrastructure* DOI: https://doi.org/10.1016/j.jmau.2016.05.001

Ishak, M.M., Deraman, M., Dolah, B.N.M, Othman, M.A.R., Omar, R., Basri, N.H., Nor, N.S.M., Taer, E., Awitdrus, A., Farma, R., and Aziz, A.A. 2015. Effects of activation time on the performance of supercapacitor binderless activated carbon electrodes derived from fibers of oil palm empty fruit bunches. *Advanced Materials Research* 1112: 308-312. DOI: https://doi.org/10.4028/www.scientific.net/AMR.1112.308

Kanjana, K., Harding, P., Kwamman, T., Kingkam, W. and Chutimasakul, T. 2021. Biomass-derived activated carbons with extremely narrow pore size distribution via eco-friendly synthesis for supercapacitor application. *Biomass and Bioenergy* 153: 106206. DOI: https://doi.org/10.1016/j.biombioe.2021.106206

Kim, Y.J., Lee, B.J., Suezaki, H., Chino, T., Abe, Y., Yanagiura, T., Park, K.C., and Endo, M. 2006. Preparation and characterization of bamboo based activated carbons as electrode materials for electric double layer capacitors. *Carbon* 44(2006): 1581-1616. DOI: https://doi.org/10.1016/j.carbon.2006.02.011

Lan, X., Jiang, X., Song, Y., Jing, X., and Xing, X. 2019. The effect of activation temperature on structure and properties of blue coke-based activated carbon by CO_2 activation. *Green Process Synth*. 8: 837-845. DOI: https://doi.org/10.1515/gps-2019-0054

Madzaki, H., Ghani, W.A.W.A.K., and Yaw, T.C.S. 2018. Carbon Dioxide Adsorption on Activated Carbon Hydrothermally Treated and Impregnated with Metal Oxides. *Jurnal Kejuruteraan* 30(1). DOI: http://dx.doi.org/10.17576/jkukm-2018-30

Mahmud, N.A., Osman, N., and Jani, A.M.M. 2018. Characterization of Acid Treated Activated Carbon from Oil Palm Empty Fruit Bunches. *IOP Conf. Series: Journal of Physics: Conf. Series* 1083. DOI: https://doi.org/10.1088/1742-6596/1083/1/012049

Mensah-Darkwa, K., Zequine, C., Kahol, P.K., and Gupta, R.K. 2019. Supercapacitor energy storage device using biowastes: A sustainable approach to green energy. *Sustainability* 11(414): 2-22. DOI: https://doi.org/10.3390/su11020414

Mopoung, S., Moonsri, P., Palas, W., and Khumpai, S. 2015. Characterization and properties of activated carbon prepared from tamarind seeds by KOH activation for Fe(III) adsorption from aqueous solution. *The Scientific World Journal*. Volume 2015. DOI: https://doi.org/10.1155/2015/415961

Najib, S., and Erdem, E. 2019. Current progress achieved in novel materials for supercapacitor electrodes: Mini review. *Nanoscale Advances* 1: 2817-2827. DOI: https://doi.org/10.1039/C9NA00345B

Nor, N.S.M., Deraman. M., Suleman, M., Jasni, M.R.M., Manjunatha, J.G., Othman, M.A.R., and Shamsudin, S.A. 2017. Supercapacitor using binderless activated carbon monoliths electordes consisting of a graphite additive and pre-carbonized biomass fibers. *International Journal of Electrochemical Science* 12(3): 2520-2539. DOI: https://doi.org/10.20964/2017.03.48

Olivares-Marin, M., Fernandez-Gonzalez, C., Macias-Garcia, A., and Gomez—Serrano, V. 2012. Preparation of activated carbon from cherry stones by physical activation in air. Influence of the chemical carbonization with H_2SO_4. *Journal of Analytical and Applied Pyrolysis* 94(2012): 131-137. DOI: https://doi.org/10.1016/j.jaap.2011.11.019

Pallares, J., Gonzalez-Cencerrado, A., and Arauz, I. 2018. Production and characterization of activated carbon from barley straw by physical activation with carbon dioxide and steam. *Biomass and Bioenergy* 115: 64-73 DOI: https://doi.org/10.1016/j.biombioe.2018.04.015

Purwanto, H., Rozhan, A.N. and Salleh, H.M. 2018. Innovative Process to Enrich Carbon Content of EFB-Derived Biochar as an Alternative Energy Source in Ironmaking. *Advances in Materials Science and Engineering*. Vol. 2018. DOI: https://doi.org/10.1155/2018/4067237

Reza, M.S., Yun, C.S., Afroze, S., Radenahmad, N., Bakar, M.S.A., Saidur, R., Taweekun, J., and Azad, A.K. 2020. Preparation of activated carbon from biomass and its' applications in water and gas purification, a review. *Arab Journal of Basic and Applied Sciences* 27(1): 208-238. DOI: https://doi.org/10.1080/25765299.2020.1766799

Sahsiny, J.J., Haizal, M.W.B., Razali, N.A.N.M., Ragunathan, T., Abdullah, S.R.S., Nordin, D., and Ali, J.M. 2021. Adsorption Efficiency Comparison of Activated Carbon Derived from Various Herbs. *Jurnal Kejuruteraan* 33(3): 593-621. DOI: https://doi.org/10.17576/jkukm-2021-33(3)-19

Shabeeba, P., Thayyil, M.S., Pillai, M.P., Soufeena, P.P. and Niveditha, C.V. 2018. Electrochemical investigation of activated carbon electrode supercapacitors. *Russian Journal of Electrochemistry* 54: 302-308. DOI: https://doi.org/10.1134/S1023193517120096

Shah, J.B., and Valaki, J.B. 2023. A Comprehensive Review on Feasibility of Different Agro Residues for Production of Bio-Oil, Bio-Char and Pyro-Gas. *Jurnal Kejuruteraan* 35(1): 77-93. DOI: https://doi.org/10.17576/jkukm-2023-35(1)-08

Shi, G., Liu, C., Wang, G., Chen, X., Li, L., Jiang, X., Zhang, P., Dong, Y., Jia, S., Tian, H. and Liu, Y. 2019. Preparation and electrochemical performance of electrospun biomass-based activated carbon nanofibers. *Ionics* 25: 1805-1812. DOI: https://doi.org/10.1007/s11581-018-2675-3

Sim, C.K., Majid, S.R., and Mahmood, N.Z., 2015. Electrochemical performance of activated carbon derived from treated food-waste. *International Journal of Electrochemical Science* 10(12): 10157-10172. DOI: https://doi.org/10.1016/S14523981(23)11250-8

Taer, E., Melisa, M., Agustino, A., Taslim, R., Sinta Mustika, W. and Apriwandi, A. 2021. Biomass-based activated carbon monolith from Tectona grandis leaf as supercapacitor electrode materials. *Energy Sources. Part A: Recovery, Utilization, and Environmental Effects* 1-12. DOI: https://doi.org/10.1080/15567036.2021.1950871

Taer, E., Taslim, R., and Deraman, M. 2016. Preparation and characterization of activated carbon monolith from rubber wood and its effect on supercapacitor performances. *AIP Conference Proceedings* 1712(1). DOI: https://doi.org/10.1063/1.4941894

Thongpat, W., Taweekun, J., and Maliwan, K. 2021. Synthesis and characterization of microporous activated carbon from rubberwood by chemical activation withKOH. *Carbon Letters* 31(2021):1079-1088. DOI: https://doi.org/10.1007/s42823-020-00224-z

Vinayagam, M., Suresh Babu, R., Sivasamy, A. and de Barros, A.L.F. 2021. Biomass-derived porous activated carbon nanofibers from Sapindus trifoliatus nut shells for high-performance symmetric supercapacitor applications. *Carbon Letters* 31(6): 1133-1143. DOI: https://doi.org/10.1007/s42823-021-00235-4

Wang, Y., Duan, Y., Liang, X., Tang, L., Sun, L., Wang, R., Wei, S., Huang, H., Yang, P., and Hu, H. 2023. Hierarchical porous activated carbon derived from coconut shell for ultrahigh-performance supercapacitors. *Molecules* 28(7187). DOI: https://doi.org/10.3390/molecules28207187

Wei, L., Tian, K., Zhang, X., Jin, Y., Shi, T. and Guo, X. 2016. 3D porous hierarchical microspheres of activated carbon from nature through nanotechnology for electrochemical double-layer capacitors. *ACS Sustainable Chemistry & Engineering* 4(12): 6463-6472. DOI: https://doi.org/10.1021/acssuschemeng.6b01227

Yang, W., Li, W., and Feng, Y. 2018. High electrochemical performance from oxygen functional groups containing porous activated carbon electrode of supercapacitors. *Materials* 11(12): 2455. DOI: https://doi.org/10.3390/ma11122455

Yu, H., Wu, J., Fan, L., Xu, K., Zhong, X., Lin, Y., and Lin, J. 2011. Improvement of the performance for quasi-solid-state supercapacitor by using PVA-KOH-KI polymer gel electrolyte. *Electrochimica Acta*. 56(20): 6881-6886. DOI: https://doi.org/10.1016/j.electacta.2011.06.039

Zheng, Y., Deng, T., Yue, N., Zhang, W., Zhu, X., Yang, H., Chu, X., and Zheng, W. 2021. Raman spectroscopy and correlative-Raman technology excel as an optimal stage for carbon-based electrode materials in electrochemical energy storage. *Journal of Raman Spectroscopy* 52(12): 2119-2130. DOI: https://doi.org/10.1002/jrs.6178

Zhi, M., Yang, F., Meng, F., Li, M., Manivannan, A., and Wu, N. 2014. Effects of pore structure on performance of an activated-carbon supercapacitor electrode recycled from scrap waste tires. *ACS Sustainable Chemistry & Engineering* 2(7): 1592-1598. DOI: https://doi.org/10.1021/sc500336h